Journal of Materials Chemistry A

ROYAL SOCIETY OF CHEMISTRY

PAPER

View Article Online
View Journal | View Issue

Cite this: J. Mater. Chem. A, 2022, 10, 16714

An acceptor with an asymmetric and extended conjugated backbone for high-efficiency organic solar cells with low nonradiative energy loss†

Jing Wang,[a] Hongbin Chen,[b] Xiaoyun Xu,[c] Zaifei Ma, *[c] Zhe Zhang,[b] Chenxi Li,[b] Yang Yang,[d] Jian Wang,[d] Yue Zhao,[e] Mingtao Zhang,[b] Xiangjian Wan,[b] Yan Lu *[a] and Yongsheng Chen *[b]

Received 17th May 2022
Accepted 19th July 2022

DOI: 10.1039/d2ta03956g

rsc.li/materials-a

One of the significant factors that limit efficiencies of organic solar cells (OSCs) is their large energy loss (E_{loss}), especially the high nonradiative recombination energy loss (ΔE_{nr}). Herein, an acceptor named NQF with an asymmetric and extended conjugation central core has been designed and synthesized. Compared with Y6, NQF exhibits upshifted HOMO and LUMO energy levels and a higher photoluminescence quantum yield (PLQY). The OSC based on PM6:NQF demonstrates a ΔE_{nr} as low as 0.177 eV and thus a high power conversion efficiency (PCE) of 17.57%. In contrast, the control device PM6:Y6 gives a PCE of 16.45% with a ΔE_{nr} value of 0.231 eV. This work achieves molecular design with low ΔE_{nr} and demonstrates that the E_{loss} of OSCs can be effectively reduced through rational and delicate molecular design.

1. Introduction

With the innovation of active layer materials, device optimization, and understanding of the mechanism, organic solar cells (OSCs) have witnessed great progress in the past decade and achieved power conversion efficiencies (PCEs) over 19%.[1–22] However, there is still a large gap between the PCEs of OSCs and other photovoltaic cells such as crystalline silicon and perovskite cells.[23–27] One of the most significant factors that limit the PCEs of OSCs is the large energy loss (E_{loss}), which originates from radiative loss and nonradiative loss.[28,29] Since the radiative loss above the bandgap is unavoidable and the radiative loss below the bandgap can be smaller than 0.10 eV for current nonfullerene acceptor based OSCs, to reduce the nonradiative loss thus has become the main strategy and focus for minimizing E_{loss} in organic photovoltaic devices.[9,28,30,31] To date, most OSCs show nonradiative loss over 0.30 eV with few examples in the range 0.20–0.30 eV,[32] which is remarkably larger than that of silicon or perovskite solar cells. In recent years, the study of nonradiative loss has become an important topic in the OSC community.[32–34] Although the detailed mechanism behind it is still not clear,[3] some valuable results have been reported based on experimental and theoretical studies.[9,27,35–39] For example, Bredas and Gao *et al.* reported that the nonradiative loss can be decreased by reducing the energy offset between the donor and acceptor and/or enhancing the luminescence efficiency of the low band gap component in the active layers.[33,40] Clearly, to minimize the nonradiative loss, the design of active layer materials always plays a crucial role.

In fact, in the past decade, the progress of OSCs was significantly driven by the invention of new active layer materials.[6,13,41–43] Among them, molecules including donors and acceptors with the acceptor–donor–acceptor (A–D–A) architecture have demonstrated great success.[44] Presently, the rapid development of nonfullerene acceptors (NFAs) with A–D–A structures such as ITIC, Y6 and their analogues and derivatives has boosted the efficiencies of OSCs to a remarkable level.[2,6,7,45–48] However, it is still a challenge to design active layer materials to address the concerns of energy loss, especially the nonradiative loss in the OSC community. As one of the most successful acceptors, Y6 has a unique banana-like

[a]School of Materials Science & Engineering, Tianjin Key Laboratory for Photoelectric Materials and Devices, Key Laboratory of Display Materials & Photoelectric Devices, Ministry of Education, Tianjin University of Technology, Tianjin 300384, China. E-mail: luyan@tjut.edu.cn

[b]State Key Laboratory of Elemento-Organic Chemistry, The Centre of Nanoscale Science and Technology, Key Laboratory of Functional Polymer Materials, College of Chemistry, Renewable Energy Conversion and Storage Center (RECAST), Nankai University, Tianjin 300071, China. E-mail: yschen99@nankai.edu.cn

[c]State Key Laboratory for Modification of Chemical Fibers and Polymer Materials, Center for Advanced Low-dimension Materials, College of Materials Science and Engineering, Donghua University, Shanghai 201620, China. E-mail: mazaifei@dhu.edu.cn

[d]The Institute of Seawater Desalination and Multipurpose Utilization, Ministry of Natural Resources (Tianjin), Tianjin 300192, China

[e]Coordination Chemistry Institute, State Key Laboratory of Coordination Chemistry, School of Chemistry and Chemical Engineering, Nanjing National Laboratory of Microstructures, Nanjing University, Nanjing 210093, China

† Electronic supplementary information (ESI) available. CCDC 2155815. For ESI and crystallographic data in CIF or other electronic format see https://doi.org/10.1039/d2ta03956g

configuration, which enables it to form an intense three-dimensional (3D) framework with efficient charge transport channels and achieves a PCE of around 16% for binary devices with E_{loss} ~ 0.55 eV and nonradiative loss ~0.22 eV.[6,49] To further improve device efficiencies, many studies have been conducted on the structural modification of Y6 on the side chains,[48,50–53] end groups,[54–58] and molecular backbones.[59–64] With the structural modifications, the molecular absorptions, energy levels and packing modes can be finely tuned, and corresponding devices with improved efficiencies over 19% have been achieved.[14–20] However, to the best of our knowledge, E_{loss} values for the vast majority of the reported devices of Y6 derivatives are still higher than 0.5 eV,[31,49,65–69] as they mainly suffer from the large nonradiative energy loss over 0.2 eV.[49,65,66,69] Thus, it is still a challenging work to minimize the nonradiative loss *via* careful molecular design.

Herein, we design and synthesize an acceptor NQF, 2,2′-((2*Z*,2′*Z*)-((16,17-bis(2-hexyldecyl)-10-oxo-3,13-diundecyl-16,17-di-hydro-10*H*-indeno[1,2-*b*]thieno[2″,3″:4′-,5′]thieno[2′,3′:4,5]pyrrolo[3,2-f]thieno[2″,3″:4′,5′]thieno[2′,3′:4,5]pyrrolo[2,3-*h*]quinoxaline-2,14-diyl)bis(methanylylidene))bis(5,6-difluoro-3-oxo-2,3-dihydro-1*H*-indene-2,1-diylidene))dimalononitrile, which has an asymmetric and extended conjugation central core compared with Y6 (Fig. 1a). The asymmetric and extended conjugation central core can increase the dipole moment of the acceptor and strengthen the rigidity of the molecule, which is expected to exhibit high luminescence efficiency and thus low nonradiative energy loss.[39,70] The binary device based on PM6:NQF shows a PCE of 17.57% with an open-circuit voltage (V_{oc}) of 0.921 V, a short-circuit current (J_{sc}) of 25.79 mA cm^{-2}, and a fill factor (FF) of 73.96%. In contrast, the control device PM6:Y6 gives a PCE of 16.45% with a V_{oc} of 0.849 V, a J_{sc} of 25.98 mA cm^{-2} and a FF of 74.56%. It is worthy of note that the higher efficiency of the NQF based device comes from its low energy loss of 0.504 eV with a remarkably low nonradiative loss of 0.177 eV, both of which are smaller than those of PM6:Y6 with the values 0.551 and 0.231 eV, respectively. These results highlight that it is a molecular design with low nonradiative recombination loss and demonstrate that the E_{loss} of OSCs can be effectively reduced through a rational and delicate molecular design.

2. Results and discussion

2.1. Synthesis and optoelectronic properties

The synthetic route of NQF is shown in Scheme S1 in the ESI.† The key intermediate compound **3** with the asymmetric backbone was synthesized *via* two steps. First the reduction of compound **1** by $LiAlH_4$ yielded compound **2**. Then compound **2** without further purification reacted with the commercially available 4,5-difluoro-1,2-phenylenediamine directly by a condensation process to offer compound **3**. The subsequent Vilsmeier–Haack reaction afforded the corresponding dialdehyde compound **4** in high yield (75%). Finally, the targeted molecule NQF was synthesized *via* Knoevenagel condensation between compound **4** and 2-(5,6-difluoro-3-oxo-2,3-dihydro-1*H*-inden-1-ylidene)malononitrile (2F-IC). The detailed synthesis procedures and characterization including ^{1}H NMR, ^{13}C NMR and mass spectra are provided in the ESI.†

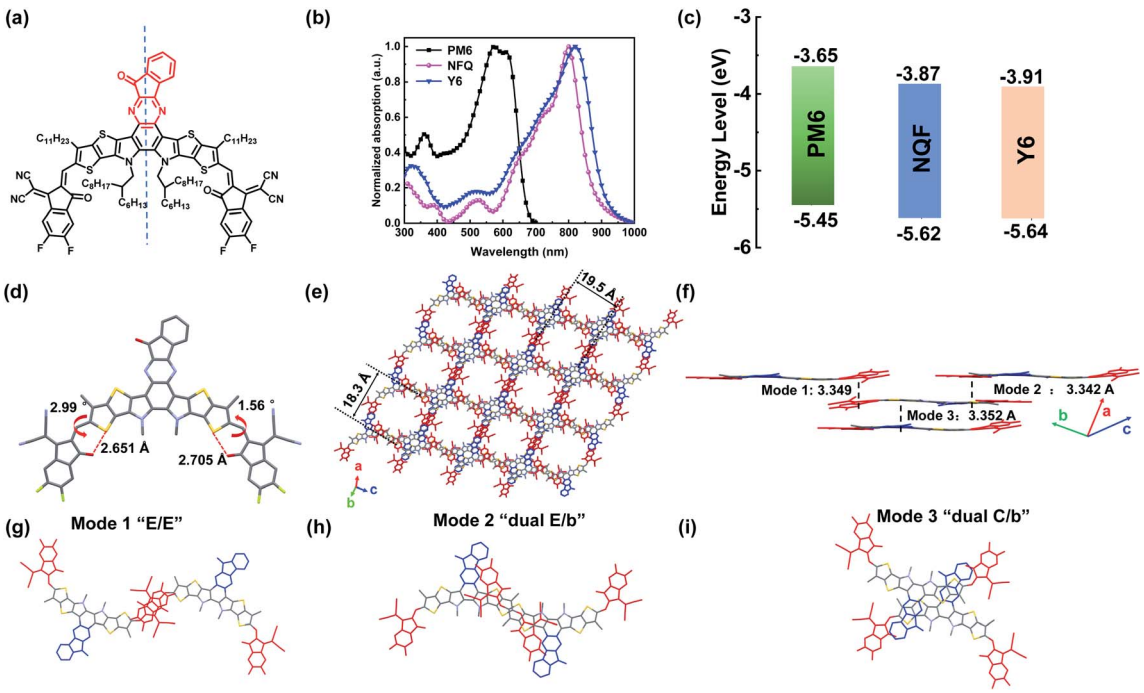

Fig. 1 (a) Chemical structure of NQF. (b) The solid film absorption spectra and (c) energy level diagram of PM6, NQF and Y6. (d) The single crystal structure of NQF from a top view. (e) The molecular packing patterns and (f–i) the three types of intermolecular packing modes in the single crystal of NQF.

The UV-vis absorption spectra of NQF and Y6 are displayed in Fig. 1b and S1 (ESI†), respectively. NQF and Y6 exhibit maximum absorption peaks at 728 nm and 733 nm in chloroform solution, and 801 and 820 nm in the film state, respectively. In contrast to their solution absorptions, the solid film absorptions of NQF and Y6 are red-shifted by 73 nm and 87 nm, respectively. Compared with Y6, NQF exhibits blue shifted absorption in solid film owing to their different packing modes. As shown in Fig. 1e, NQF shows two-dimensional (2D) arrangement *via* π–π stacking, however, Y6 shows a 3D network in a single crystal structure.[71] The UV-vis spectra of the two blend films PM6:NQF and PM6:Y6 are presented in Fig. S2 (ESI†). It can be found that the two blend films show two peaks corresponding to PM6 and the acceptors. Clearly, in the acceptor absorption range, a slight blue shift is observed for NQF compared with Y6, which is consistent with their neat films. The solubilities of Y6 and NQF in chloroform were measured by the UV-vis method[72,73] and the results are listed in Table S1 (ESI†). The solubility of NQF in chloroform is about 389.26 mg mL^{-1}, which is significantly higher than that of Y6 in chloroform (47.68 mg mL^{-1}). The energy levels of NQF were investigated by cyclic voltammetry (CV). From the onset reduction and oxidation potentials of the CV curves (Fig. S3, ESI†), the lowest unoccupied molecular orbital (LUMO) and the highest occupied molecular orbital (HOMO) levels of NQF were estimated to be −3.87 and −5.62 eV, respectively, which are all upshifted compared with those of Y6 after introducing the asymmetric central unit (Fig. 1c). The upshifted energy levels of NQF should decrease the energy offset with PM6 and thus a higher V_{oc} with suppressed radiative loss is expected according to the results reported by Gao *et al.*[40]

The single crystal of NQF was obtained by diffusing methanol into the chloroform solution of NQF. The related parameters of NQF X-ray data are listed in Table S2.† As shown in Fig. 1d, NQF exhibits a banana-like configuration with the non-covalent S–O interaction to form conformational locks. The twist angles between the end groups and core of NQF are 1.56° and 2.99°, indicating the good planarity of the acceptor. Unlike the single crystal structure of Y6 with the 3D network,[71] NQF shows two-dimensional (2D) arrangement *via* π–π stacking in the crystal and forms square-shaped voids with a side length of ~18.3 × 19.5 Å (Fig. 1e). The crystal structure of the NQF molecule exhibits three types of intermolecular packing modes with intense π–π stacking (Fig. 1f–i), *i.e.* the end group to end group mode ("E/E" mode), dual end group to the thieno[3,2-*b*] thiophene unit mode ("dual E/b" mode) and dual central unit to the thieno[3,2-*b*]thiophene unit mode ("dual C/b" mode).[74] NQF demonstrates end group to end group π–π stacking (*J*-aggregation) with a distance of 3.35 Å (Fig. 1g), which is compared with that of the single-crystal of Y6.[71]

2.2. Photovoltaic performance

The OSC devices with the conventional structure of ITO/PEDOT:PSS/PM6:NQF/PDINO/Ag (Fig. 2a) were fabricated to evaluate the photovoltaic performance of NQF. The wide-bandgap polymer PM6 was selected as the donor owing to its matching energy levels and complementary absorption with NQF.[75] Detailed device fabrication and optimization conditions are provided in Table S3 (ESI†). The current density–voltage (*J*–*V*) curves of the optimal devices together with PM6:Y6 for comparison are illustrated in Fig. 2b, and their corresponding photovoltaic parameters are summarized in Table 1. The optimized device based on NQF gave a high PCE of 17.57% with a notably high V_{oc} of 0.921 V, a J_{sc} of 25.79 mA cm^{-2} and a FF of 73.96%. In contrast, the control device PM6:Y6 showed a PCE of 16.45% with a V_{oc} of 0.849 V, a J_{sc} of 25.98 mA cm^{-2} and a FF of 74.56%. Clearly, these two types of devices have rather comparable J_{sc} and FF but significantly different V_{oc}. The enhanced efficiency of the device based on NQF is thus ascribed to its remarkably larger V_{oc} mainly owing to the small energy loss as will be discussed below. As shown in Fig. 2c, the external quantum efficiency (EQE) curves of the two devices featured high photon responses covering the range of 300 to 900 nm. The calculated J_{sc} values from the EQE curves of the devices based on NQF and Y6 are 24.86 mA cm^{-2} and 24.99 mA cm^{-2}, respectively, which are in good agreement with the J_{sc} measured from the *J*–*V* curves.

2.3. E_{loss} analysis

The OSC based on NQF shows a notably high V_{oc} of 0.921 V compared with that of the device based on Y6 with a value of 0.849 V. To investigate the reason behind it, the detailed E_{loss} analysis was conducted. The E_{loss} values of the two devices were calculated using the equation $E_{loss} = E_{gap} - qV_{oc}$, where the E_{gap} values were estimated by the intersections between the

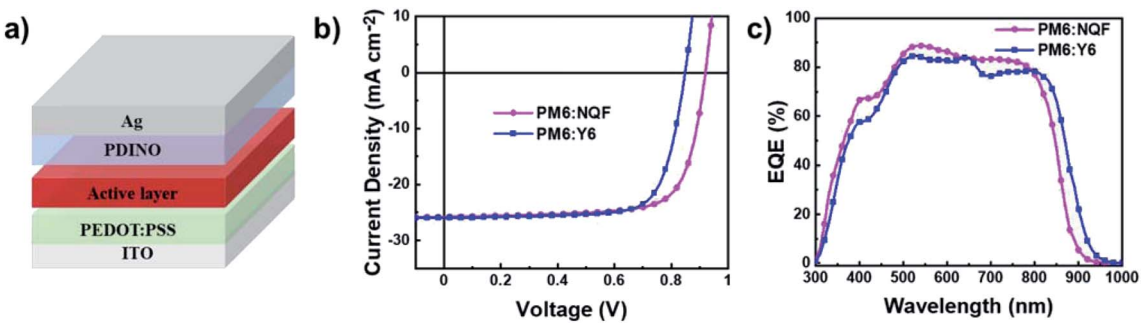

Fig. 2 (a) The device structure. (b) *J*–*V* curves and (c) EQE curves of the optimized devices of PM6:NQF and PM6:Y6.

Table 1 Summary of device parameters of the optimized OSCs[a]

Active layer	V_{oc} (V)	J_{sc} (mA cm^{-2})	Calc. J_{sc}[b] (mA cm^{-2})	FF (%)	PCE (%)
PM6:NQF	0.921 (0.918 ± 0.003)	25.79 (25.32 ± 0.40)	24.86	73.96 (73.84 ± 1.18)	17.57 (17.17 ± 0.16)
PM6:Y6	0.849 (0.844 ± 0.004)	25.98 (25.82 ± 0.51)	24.99	74.56 (73.96 ± 0.97)	16.45 (16.07 ± 0.40)

[a] Optimal and statistical results are listed outside of parentheses and in parentheses, respectively. The average parameters were calculated from 15 independent devices. [b] J_{sc} calculated from EQE curves.

absorption and emission spectra of the low bandgap component NQF and Y6 (Fig. S6, ESI†).[76] As summarized in Table 2, the OSC based on NQF exhibited a E_{loss} of 0.504 eV, which is remarkably lower than that of PM6:Y6 with the value of 0.551 eV and among the lowest E_{loss} values for high efficiency OSCs. Next, the detailed E_{loss} components were investigated following the reported methods. In OSCs, the E_{loss} can be divided into three parts: $E_{loss} = \Delta E_1 + \Delta E_2 + \Delta E_3$, where ΔE_1 is the radiative recombination loss above the bandgap, ΔE_2 is the radiative recombination loss below the bandgap and ΔE_3 is the nonradiative energy loss.[28,77] According to the Shockley–Queisser (SQ) theory, ΔE_1 is unavoidable for any type of solar cells and is generally 0.25–0.3 eV.[67] Here, the device PM6:NQF shows the ΔE_1 value of 0.264 eV, comparable with that of the Y6 based device (0.262 eV). ΔE_2 can be calculated according to the following equation: $\Delta E_2 = q(V_{oc,sq} - V_{oc,rad})$, where $V_{oc,sq}$ is the maximum V_{oc} according to the SQ theory.[78] $V_{oc,rad}$ is the V_{oc} when there is only radiative recombination in the OSC, which can be determined by highly sensitive external quantum efficiency (sEQE) and EL measurements (Fig. 3a and b, the details for the determination of $V_{oc,rad}$ are presented in the ESI†).[76,79] The third part ΔE_3, also named nonradiative recombination

Table 2 Energy loss analysis of PM6:NQF and PM6:Y6 based devices

Active layer	V_{oc} (V)	E_g[a] (eV)	E_{loss} (V)	$V_{oc,sq}$[b] (V)	ΔE_1[c] (eV)	$V_{oc,rad}$[d] (V)	ΔE_2 (eV)	ΔE_3 (cal. V)	EQE_{EL}	ΔE_3 (exp. V)
PM6:NQF	0.921	1.425	0.504	1.161	0.264	1.073	0.088	0.152	8.4×10^{-4}	0.177
PM6:Y6	0.849	1.400	0.551	1.138	0.262	1.043	0.095	0.194	9.6×10^{-5}	0.231

[a] E_g was estimated *via* the crossing points between normalized absorption and PL spectra of films. [b] $V_{oc,sq}$ is calculated according to the SQ limit. [c] $\Delta E_1 = E_g - V_{oc,sq}$. [d] $V_{oc,rad}$ is the V_{oc} when there is only radiative recombination and are calculated from EL and sEQE measurements. ΔE_3 ($\Delta E_3 = q\Delta V_{nr}$) is determined by two approaches: (1) calculated from $q(V_{oc,rad} - V_{oc})$ and (2) obtained from the equation $q\Delta V_{nr} = -kT \ln EQE_{EL}$ by measuring the device EQE_{EL}.

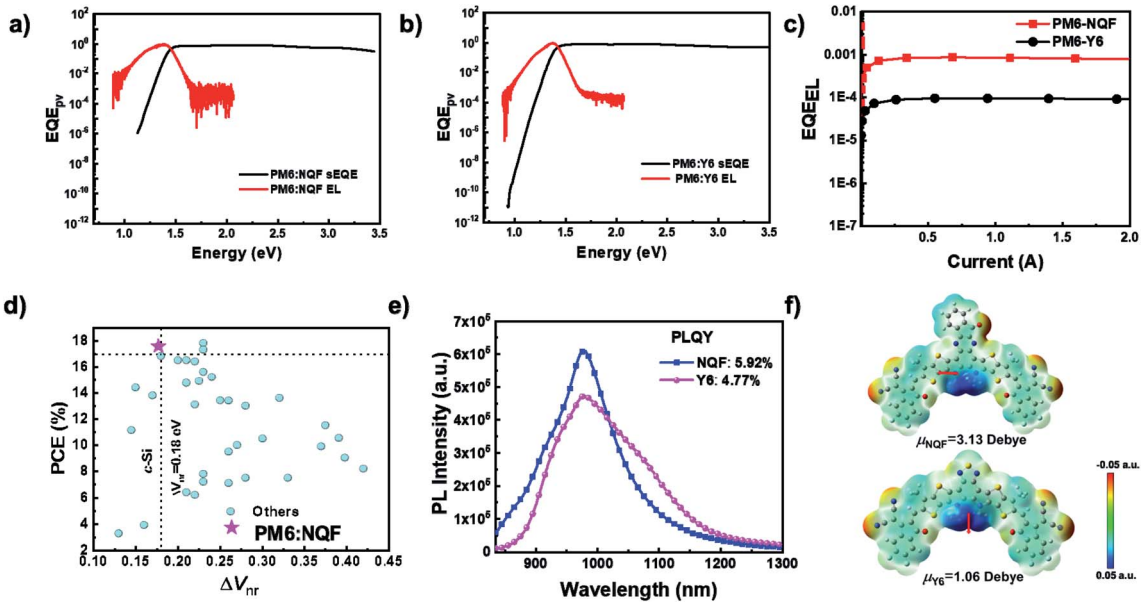

Fig. 3 (a and b) EQE_{PV} curves of PM6:NQF and PM6:Y6. (c) EQE_{EL} spectra of PM6:NQF and PM6:Y6. (d) Published statistics: ΔV_{nr} *versus* PCE. (e) Photoluminescence spectra of the NQF and Y6 films together with their quantum efficiencies. (f) DFT (B3LYP/6-31G(d)) calculated electrostatic charge distributions and dipole moments for NQF and Y6.

energy loss (ΔE_{nr}), is the determined factor of energy loss for OSCs, which originates from the nonradiative decay of the charge transfer states and recombination of free charges. ΔE_3 can be calculated from the EQE of EL (EQE_{EL}) following the equation $\Delta E_3 = -kT\ln(EQE_{EL})$.[80] As illustrated in Fig. 3c and summarized in Table 2, the device based on NQF exhibits about one order higher EQE_{EL} (8.4×10^{-4}) than the Y6 based device (9.60×10^{-5}), corresponding to a notably smaller ΔE_3 value of 0.177 eV. To our knowledge, it is the lowest nonradiative energy loss for binary OSCs with PCE over 17% (Fig. 3d, detailed published statistics as shown in Table S4 in the ESI†).

According to the research results reported by Bredas and Gao *et al.*,[40] the photoluminescence efficiencies of the pristine material components define the limit of ΔV_{nr} in organic solar cells, and the higher photoluminescence efficiency of the low band gap component in the active layer favors a lower ΔV_{nr}. In our case, NQF shows a higher photoluminescence quantum yield (PLQY) (5.92%) than Y6 (4.77%) (Fig. 3e and S7, ESI†). In addition, the EQE_{EL} values of corresponding pure-phase devices were also measured (Fig. S8, ESI†). The NQF based device exhibits a much higher EQE_{EL} (6.7×10^{-4}) than the Y6 based device (1.2×10^{-4}), which is consistent with the higher photoluminescence efficiency of NQF. The higher PLQY of NQF should originate from its asymmetric and extended conjugation structure. According to the theoretical calculations at the B3LYP/6-31G(d) level, the asymmetrical structure of NQF possesses a stronger electrostatic charge distribution difference in the asymmetrical central core, leading to a higher dipole moment, 3.13 debye for NQF *vs.* 1.06 debye for Y6 (Fig. 3f). The higher dipole moment for NQF can enhance *J*-aggregation in the solid film.[39,70] This is consistent with the results in the single crystal and GIWAXS. The enhanced *J*-aggregation favors high luminescence efficiencies according to the established results in the organic optoelectronics.[70] In addition, the EL values of the pure NQF and Y6 film were also measured. As shown in Fig. S9 (ESI†), the EL spectra of pure NQF and Y6 nearly overlapped with their corresponding blending films with PM6, especially for the NQF system.

2.4. Charge transport, exciton dissociation and charge generation

The properties of the charge transport, exciton dissociation and charge generation of the two devices based on NQF and Y6 were studied side by side for comparison. The space-charge-limited current (SCLC) method was employed to measure the charge mobilities of the blend films of PM6:Y6 and PM6:NQF. As shown in Fig. S10 (ESI†), the electron/hole mobilities were calculated to be $5.00 \times 10^{-4}/3.31 \times 10^{-4}$ and $4.39 \times 10^{-4}/1.52 \times 10^{-4}$ cm^{-2} V^{-1} s^{-1} for the PM6:Y6 and PM6:NQF based devices, respectively. The comparable values of electron mobilities for the two devices indicate that the PM6:NQF based device has similar charge transport ability to that of the Y6 based device. Furthermore, in order to investigate the exciton dissociation and charge generation properties, the dependence of photocurrent density (J_{ph}) on the effective voltage (V_{eff}) was measured for the two devices (Fig. S11, ESI†). The exciton dissociation probabilities (P_{diss}), calculated from J_{ph} under the short-circuit conditions divided by the saturated photocurrent density (J_{sat}), were 96.21% and 96.47% for NQF and Y6 based devices, respectively, demonstrating the highly efficient exciton dissociation for the two devices. To study the behavior of charge recombination of the two devices, the plots of light-intensity dependence (P) of J_{sc} ($J_{sc} \propto P^{\alpha}$), where the exponent α being close to 1 reflects a weak bimolecular recombination, were measured and are displayed in Fig. S12 (ESI†). The J_{sc} values of NQF and Y6 based devices were highly linearly correlated with P, with the α values of 0.982 and 0.989, respectively, illustrating that the two devices based on NQF and Y6 all showed efficient charge dissociation and less bimolecular recombination.

2.5. Morphology analysis

The morphologies of PM6:NQF together with PM:Y6 for comparison were characterized by atomic force microscopy (AFM) and transmission electron microscopy (TEM). As illustrated in Fig. S13 (ESI†), the two blend films showed smooth surface morphologies with fibrillar networks. The root-mean-square roughness (R_q) values are 1.22 and 1.05 nm for NQF and Y6 based blend films, respectively. The interpenetrating network with nanoscale phase separation could also be seen in the TEM images (Fig. S14, ESI†). The results indicate that the structural modulation of Y6 *via* introducing the asymmetric core could yield favorable morphology like the Y6 based blend film.

Grazing incidence wide-angle X-ray scattering (GIWAXS) was used to investigate the molecular stacking and orientation of NQF and its blend film with PM6. As shown in Fig. 4, the neat film of NQF shows a clear lamellar stacking peak at 0.46 $Å^{-1}$ with a *d* spacing of 13.78 Å and a strong π–π stacking diffraction peak (010) at 1.73 $Å^{-1}$ with a *d* spacing of 3.63 Å in the out of plane (OOP) direction, indicating a face-on orientation. Compared with the pattern parameters of Y6 measured under the same conditions (Table S5, ESI†), NQF has a relatively smaller CCL both in the (010) OOP and (100) IP directions, which indicates a slightly weak crystallinity and is consistent with the crystal packing modes of Y6 and NQF. The blend films of PM6:NQF and PM6:Y6 all exhibit a face-on orientation with

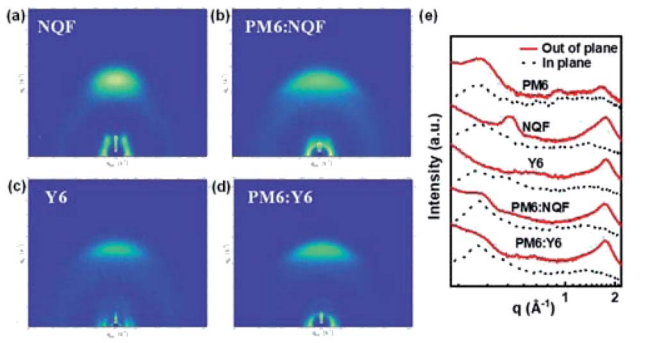

Fig. 4 (a–d) 2D GIWAXS patterns for pure NQF film, pure Y6 film, PM6:NQF blend film and PM6:Y6 blend film, respectively. (e) In-plane and out-of-plane line cuts of the corresponding GIWAXS patterns.

strong π–π stacking diffraction peaks (010) in the OOP direction and lamellar diffraction peaks (100) in the IP direction. The π–π stacking *d* spacing in PM6:NQF is 3.65 Å, comparable with that in the blend film of Y6 (3.61 Å). As shown in Table S5,† compared with that of PM6:Y6, the blend film of NQF shows a relatively smaller CCL with a value of 21.01 Å in the (010) OOP and slightly larger CCL with a value of 92.70 Å in the (100) IP direction.

3. Conclusions

In summary, we designed an acceptor NQF with an asymmetric and extended backbone. Compared with Y6, NQF exhibits upshifted HOMO and LUMO energy levels, which reduces the energy offset with the PM6 donor. Meanwhile, NQF shows a higher PLQY owing to its asymmetric, extended and rigid conjugation structure. Thus, PM6:NQF based OSC demonstrates a high EQE_{EL} of 8.39×10^{-4}, corresponding to a nonradiative energy loss as low as 0.177 eV. With this, the OSCs based on PM6:NQF achieved a PCE of 17.57% with a significantly higher V_{oc} of 0.921 V and almost the same J_{sc} and FF compared with the control Y6 based device. Our results show the very promising role of acceptors with an asymmetric and extended conjugation core and its impacts on the molecular packing, luminescence properties and nonradiative energy loss. This might offer some new opportunities to design high-efficiency materials with low nonradiative loss. It is also believed that the nonradiative energy loss in OSCs can be further reduced *via* chemical structure modification of the active layer materials, and OSCs with efficiencies comparable to those of inorganic solar cells can be realized in the near future.

Conflicts of interest

There are no conflicts of interest to declare.

Acknowledgements

The authors gratefully acknowledge the financial support from NSFC (52173010, 51603149 and 21935007), MoST (2019YFA0705900) of China, 111 Project (B12015) and the Haihe Laboratory of Sustainable Chemical Transformations.

Notes and references

1 Y.-J. Cheng, S.-H. Yang and C.-S. Hsu, *Chem. Rev.*, 2009, **109**, 5868–5923.
2 Y. Lin, J. Wang, Z.-G. Zhang, H. Bai, Y. Li, D. Zhu and X. Zhan, *Adv. Mater.*, 2015, **27**, 1170–1174.
3 J. Hou, O. Inganas, R. H. Friend and F. Gao, *Nat. Mater.*, 2018, **17**, 119–128.
4 W. Zhao, S. Zhang, Y. Zhang, S. Li, X. Liu, C. He, Z. Zheng and J. Hou, *Adv. Mater.*, 2018, **30**, 1704837.
5 H. Yan, Y. Tang, X. Sui, Y. Liu, B. Gao, X. Liu, S. F. Liu, J. Hou and W. Ma, *ACS Energy Lett.*, 2019, **4**, 1356–1363.
6 J. Yuan, Y. Zhang, L. Zhou, G. Zhang, H.-L. Yip, T.-K. Lau, X. Lu, C. Zhu, H. Peng, P. A. Johnson, M. Leclerc, Y. Cao, J. Ulanski, Y. Li and Y. Zou, *Joule*, 2019, **3**, 1140–1151.
7 Q. Liu, Y. Jiang, K. Jin, J. Qin, J. Xu, W. Li, J. Xiong, J. Liu, Z. Xiao, K. Sun, S. Yang, X. Zhang and L. Ding, *Sci. Bull.*, 2020, **65**, 272–275.
8 Y. Lin, Y. Firdaus, F. H. Isikgor, M. I. Nugraha, E. Yengel, G. T. Harrison, R. Hallani, A. El-Labban, H. Faber, C. Ma, X. Zheng, A. Subbiah, C. T. Howells, O. M. Bakr, I. McCulloch, S. De Wolf, L. Tsetseris and T. D. Anthopoulos, *ACS Energy Lett.*, 2020, **5**, 2935–2944.
9 N. An, Y. Cai, H. Wu, A. Tang, K. Zhang, X. Hao, Z. Ma, Q. Guo, H. S. Ryu, H. Y. Woo, Y. Sun and E. Zhou, *Adv. Mater.*, 2020, **32**, 2002122.
10 L. Liu, S. Chen, Y. Qu, X. Gao, L. Han, Z. Lin, L. Yang, W. Wang, N. Zheng, Y. Liang, Y. Tan, H. Xia and F. He, *Adv. Mater.*, 2021, **33**, 2101279.
11 Y. Liu, J. Song and Z. Bo, *Chem. Commun.*, 2021, **57**, 302–314.
12 Y. Qin, Y. Chang, X. Zhu, X. Gu, L. Guo, Y. Zhang, Q. Wang, J. Zhang, X. Zhang, X. Liu, K. Lu, E. Zhou, Z. Wei and X. Sun, *Nano Today*, 2021, **41**, 101289.
13 Y. Sun, H.-H. Gao, S. Wu, L. Meng, X. Wan, M. Li, Z. Ma, Z. Guo, S. Li, H. Zhang, C. Li and Y. Chen, *Sci. China: Chem.*, 2021, **64**, 608–615.
14 P. Bi, S. Zhang, Z. Chen, Y. Xu, Y. Cui, T. Zhang, J. Ren, J. Qin, L. Hong, X. Hao and J. Hou, *Joule*, 2021, **5**, 2408–2419.
15 Y. Cui, Y. Xu, H. Yao, P. Bi, L. Hong, J. Zhang, Y. Zu, T. Zhang, J. Qin, J. Ren, Z. Chen, C. He, X. Hao, Z. Wei and J. Hou, *Adv. Mater.*, 2021, **33**, 2102420.
16 K. Chong, X. Xu, H. Meng, J. Xue, L. Yu, W. Ma and Q. Peng, *Adv. Mater.*, 2022, **34**, 2109516.
17 R. Sun, Y. Wu, X. Yang, Y. Gao, Z. Chen, K. Li, J. Qiao, T. Wang, J. Guo, C. Liu, X. Hao, H. Zhu and J. Min, *Adv. Mater.*, 2022, **34**, 2110147.
18 C. He, Y. Pan, Y. Ouyang, Q. Shen, Y. Gao, K. Yan, J. Fang, Y. Chen, C.-Q. Ma, J. Min, C. Zhang, L. Zuo and H. Chen, *Energy Environ. Sci.*, 2022, **15**, 2537–2544.
19 L. Zhu, M. Zhang, J. Xu, C. Li, J. Yan, G. Zhou, W. Zhong, T. Hao, J. Song, X. Xue, Z. Zhou, R. Zeng, H. Zhu, C.-C. Chen, R. C. I. MacKenzie, Y. Zou, J. Nelson, Y. Zhang, Y. Sun and F. Liu, *Nat. Mater.*, 2022, **21**, 656–663.
20 Y. Wei, Z. Chen, G. Lu, N. Yu, C. Li, J. Gao, X. Gu, X. Hao, G. Lu, Z. Tang, J. Zhang, Z. Wei, X. Zhang and H. Huang, *Adv. Mater.*, 2022, 2204718.
21 S. Li, Q. Fu, L. Meng, X. Wan, L. Ding, G. Lu, G. Lu, Z. Yao, C. Li and Y. Chen, *Angew. Chem., Int. Ed.*, 2022, e202207397.
22 P. Li, X. Meng, K. Jin, Z. Xu, J. Zhang, L. Zhang, C. Niu, F. Tan, C. Yi, Z. Xiao, Y. Feng, G.-W. Wang and L. Ding, *Carbon Energy*, 2022, 1–11.
23 K. Vandewal, Z. Ma, J. Bergqvist, Z. Tang, E. Wang, P. Henriksson, K. Tvingstedt, M. R. Andersson, F. Zhang and O. Inganas, *Adv. Funct. Mater.*, 2012, **22**, 3480–3490.
24 S. M. Menke, N. A. Ran, G. C. Bazan and R. H. Friend, *Joule*, 2018, **2**, 25–35.
25 D. Qian, Z. Zheng, H. Yao, W. Tress, T. R. Hopper, S. Chen, S. Li, J. Liu, S. Chen, J. Zhang, X.-K. Liu, B. Gao, L. Ouyang, Y. Jin, G. Pozina, I. A. Buyanova, W. M. Chen, O. Inganas,

V. Coropceanu, J.-L. Bredas, H. Yan, J. Hou, F. Zhang, A. A. Bakulin and F. Gao, *Nat. Mater.*, 2018, **17**, 703–709.
26 V. C. Nikolis, A. Mischok, B. Siegmund, J. Kublitski, X. Jia, J. Benduhn, U. Hoermann, D. Neher, M. C. Gather, D. Spoltore and K. Vandewal, *Nat. Commun.*, 2019, **10**, 3706.
27 S. Liu, J. Yuan, W. Deng, M. Luo, Y. Xie, Q. Liang, Y. Zou, Z. He, H. Wu and Y. Cao, *Nat. Photonics*, 2020, **14**, 300–305.
28 J. Liu, S. Chen, D. Qian, B. Gautam, G. Yang, J. Zhao, J. Bergqvist, F. Zhang, W. Ma, H. Ade, O. Inganas, K. Gundogdu, F. Gao and H. Yan, *Nat. Energy*, 2016, **1**, 16089.
29 Y. Wang, D. Qian, Y. Cui, H. Zhang, J. Hou, K. Vandewal, T. Kirchartz and F. Gao, *Adv. Energy Mater.*, 2018, **8**, 1801352.
30 O. D. Miller, E. Yablonovitch and S. R. Kurtz, *IEEE J. Photovoltaics*, 2012, **2**, 303–311.
31 R. Yu, H. Yao, Y. Cui, L. Hong, C. He and J. Hou, *Adv. Mater.*, 2019, **31**, 1902302.
32 X. Liu, X. Du, J. Wang, C. Duan, X. Tang, T. Heumueller, G. Liu, Y. Li, Z. Wang, J. Wang, F. Liu, N. Li, C. J. Brabec, F. Huang and Y. Cao, *Adv. Energy Mater.*, 2018, **8**, 1801699.
33 X.-K. Chen and J.-L. Bredas, *Adv. Energy Mater.*, 2018, **8**, 1702227.
34 S. Xie, Y. Xia, Z. Zheng, X. Zhang, J. Yuan, H. Zhou and Y. Zhang, *Adv. Funct. Mater.*, 2018, **28**, 1705659.
35 F. D. Eisner, M. Azzouzi, Z. Fei, X. Hou, T. D. Anthopoulos, T. J. S. Dennis, M. Heeney and J. Nelson, *J. Am. Chem. Soc.*, 2019, **141**, 6362–6374.
36 G. Han and Y. Yi, *J. Phys. Chem. Lett.*, 2019, **10**, 2911–2918.
37 Y. Qin, S. Zhang, Y. Xu, L. Ye, Y. Wu, J. Kong, B. Xu, H. Yao, H. Ade and J. Hou, *Adv. Energy Mater.*, 2019, **9**, 1901823.
38 K. D. Rosenthal, M. P. Hughes, B. R. Luginbuhl, N. A. Ran, A. Karki, S.-J. Ko, H. Hu, M. Wang, H. Ade and N. Thuc-Quyen, *Adv. Energy Mater.*, 2019, **9**, 1901077.
39 W. Liu, S. Sun, L. Zhou, Y. Cui, W. Zhang, J. Hou, F. Liu, S. Xu and X. Zhu, *Angew. Chem., Int. Ed.*, 2022, e202116111.
40 X.-K. Chen, D. Qian, Y. Wang, T. Kirchartz, W. Tress, H. Yao, J. Yuan, M. Huelsbeck, M. Zhang, Y. Zou, Y. Sun, Y. Li, J. Hou, O. Inganas, V. Coropceanu, J.-L. Bredas and F. Gao, *Nat. Energy*, 2021, **6**, 799–806.
41 X. Ke, L. Meng, X. Wan, M. Li, Y. Sun, Z. Guo, S. Wu, H. Zhang, C. Li and Y. Chen, *J. Mater. Chem. A*, 2020, **8**, 9726–9732.
42 Y. Ma, M. Zhang, S. Wan, P. Yin, P. Wang, D. Cai, F. Liu and Q. Zheng, *Joule*, 2021, **5**, 197–209.
43 C. Tang, X. Ma, J.-Y. Wang, X. Zhang, R. Liao, Y. Ma, P. Wang, P. Wang, T. Wang, F. Zhang and Q. Zheng, *Angew. Chem., Int. Ed.*, 2021, **60**, 19314–19323.
44 X. Wan, C. Li, M. Zhang and Y. Chen, *Chem. Soc. Rev.*, 2020, **49**, 2828–2842.
45 S. Dai, F. Zhao, Q. Zhang, T.-K. Lau, T. Li, K. Liu, Q. Ling, C. Wang, X. Lu, W. You and X. Zhan, *J. Am. Chem. Soc.*, 2017, **139**, 1336–1343.
46 W. Zhao, S. Li, H. Yao, S. Zhang, Y. Zhang, B. Yang and J. Hou, *J. Am. Chem. Soc.*, 2017, **139**, 7148–7151.
47 W. Gao, H. Fu, Y. Li, F. Lin, R. Sun, Z. Wu, X. Wu, C. Zhong, J. Min, J. Luo, H. Y. Woo, Z. Zhu and A. K. Y. Jen, *Adv. Energy Mater.*, 2021, **11**, 2003177.
48 C. Li, J. Zhou, J. Song, J. Xu, H. Zhang, X. Zhang, J. Guo, L. Zhu, D. Wei, G. Han, J. Min, Y. Zhang, Z. Xie, Y. Yi, H. Yan, F. Gao, F. Liu and Y. Sun, *Nat. Energy*, 2021, **6**, 605–613.
49 Y. Cui, H. Yao, J. Zhang, T. Zhang, Y. Wang, L. Hong, K. Xian, B. Xu, S. Zhang, J. Peng, Z. Wei, F. Gao and J. Hou, *Nat. Commun.*, 2019, **10**, 2515.
50 Y. Cui, H. Yao, J. Zhang, K. Xian, T. Zhang, L. Hong, Y. Wang, Y. Xu, K. Ma, C. An, C. He, Z. Wei, F. Gao and J. Hou, *Adv. Mater.*, 2020, **32**, 1908205.
51 A. M. H. Cheung, H. Yu, S. Luo, Z. Wang, Z. Qi, W. Zhou, L. Arunagiri, Y. Chang, H. Yao, H. Ade and H. Yan, *J. Mater. Chem. A*, 2020, **8**, 23239–23247.
52 C. Kim, S. Chen, J. S. Park, G.-U. Kim, H. Kang, S. Lee, P. Tan Ngoc-Lan, S.-K. Kwon, Y.-H. Kim and B. J. Kim, *J. Mater. Chem. A*, 2021, **9**, 24622–24630.
53 Z. Li, C. Zhu, J. Yuan, L. Zhou, W. Liu, X. Xia, J. Hong, H. Chen, Q. Wei, X. Lu, Y. Li and Y. Zou, *J. Energy Chem.*, 2022, **65**, 173–178.
54 Y. Li, Y. Cai, Y. Xie, J. Song, H. Wu, Z. Tang, J. Zhang, F. Huang and Y. Sun, *Energy Environ. Sci.*, 2021, **14**, 5009–5016.
55 C. Cao, H. Lai, H. Chen, Y. Zhu, M. Pu, N. Zheng and F. He, *J. Mater. Chem. A*, 2021, **9**, 16418–16426.
56 Y. Pan, X. Zheng, J. Guo, Z. Chen, S. Li, C. He, S. Ye, X. Xia, S. Wang, X. Lu, H. Zhu, J. Min, L. Zuo, M. Shi and H. Chen, *Adv. Funct. Mater.*, 2021, **32**, 2108614.
57 C. He, Z. Bi, Z. Chen, J. Guo, X. Xia, X. Lu, J. Min, H. Zhu, W. Ma, L. Zuo and H. Chen, *Adv. Funct. Mater.*, 2022, 2112511.
58 L. Wang, Q. An, L. Yan, H.-R. Bai, M. Jiang, A. Mahmood, C. Yang, H. Zhi and J.-L. Wang, *Energy Environ. Sci.*, 2022, **15**, 320–333.
59 W. Liu, J. Zhang, S. Xu and X. Zhu, *Sci. Bull.*, 2019, **64**, 1144–1147.
60 C. Zhu, K. An, W. Zhong, Z. Li, Y. Qian, X. Su and L. Ying, *Chem. Commun.*, 2020, **56**, 4700–4703.
61 Y. Zhao, H. Chen, C. Zhu, J. Yuan, Y. Li, J. Hai, Y. Hu, L. Jiang, G. Chen and Y. Zou, *Mater. Chem. Front.*, 2020, **4**, 3310–3318.
62 C. Zhu, J. Yuan, F. Cai, L. Meng, H. Zhang, H. Chen, J. Li, B. Qiu, H. Peng, S. Chen, Y. Hu, C. Yang, F. Gao, Y. Zou and Y. Li, *Energy Environ. Sci.*, 2020, **13**, 2459–2466.
63 Z. Zhou, W. Liu, G. Zhou, M. Zhang, D. Qian, J. Zhang, S. Chen, S. Xu, C. Yang, F. Gao, H. Zhu, F. Liu and X. Zhu, *Adv. Mater.*, 2020, **32**, 1906324.
64 F. Lin, K. Jiang, W. Kaminsky, Z. Zhu and A. K. Y. Jen, *J. Am. Chem. Soc.*, 2020, **142**, 15246–15251.
65 J. Yuan, T. Huang, P. Cheng, Y. Zou, H. Zhang, J. L. Yang, S.-Y. Chang, Z. Zhang, W. Huang, R. Wang, D. Meng, F. Gao and Y. Yang, *Nat. Commun.*, 2019, **10**, 570.
66 X. Ma, J. Wang, J. Gao, Z. Hu, C. Xu, X. Zhang and F. Zhang, *Adv. Energy Mater.*, 2020, **10**, 2001404.
67 S. Li, L. Zhan, Y. Jin, G. Zhou, T.-K. Lau, R. Qin, M. Shi, C.-Z. Li, H. Zhu, X. Lu, F. Zhang and H. Chen, *Adv. Mater.*, 2020, **32**, 2001160.

68 Q. Liu, Y. Wang, J. Fang, H. Liu, L. Zhu, X. Guo, M. Gao, Z. Tang, L. Ye, F. Liu, M. Zhang and Y. Li, *Nano Energy*, 2021, **85**, 105963.
69 H. Xia, Y. Zhang, W. Deng, K. Liu, X. Xia, C.-J. Su, U. S. Jeng, M. Zhang, J. Huang, J. Huang, C. Yan, W.-Y. Wong, X. Lu, W. Zhu and G. Li, *Adv. Mater.*, 2022, 2107659.
70 N. J. Hestand and F. C. Spano, *Chem. Rev.*, 2018, **118**, 7069–7163.
71 W. Zhu, A. P. Spencer, S. Mukherjee, J. M. Alzola, V. K. Sangwan, S. H. Amsterdam, S. M. Swick, L. O. Jones, M. C. Heiber, A. A. Herzing, G. Li, C. L. Stern, D. M. DeLongchamp, K. L. Kohlstedt, M. C. Hersam, G. C. Schatz, M. R. Wasielewski, L. X. Chen, A. Facchetti and T. J. Marks, *J. Am. Chem. Soc.*, 2020, **142**, 14532–14547.
72 B. Walker, A. Tamayo, D. T. Duong, X.-D. Dang, C. Kim, J. Granstrom and T.-Q. Nguyen, *Adv. Energy Mater.*, 2011, **1**, 221–229.
73 G. R. He, Z. Li, X. J. Wan, J. Y. Zhou, G. K. Long, S. Z. Zhang, M. T. Zhang and Y. S. Chen, *J. Mater. Chem. A*, 2013, **1**, 1801–1809.
74 H. Chen, Y. Zou, H. Liang, T. He, X. Xu, Y. Zhang, Z. Ma, J. Wang, M. Zhang, Q. Li, C. Li, G. Long, X. Wan, Z. Yao and Y. Chen, *Sci. China: Chem.*, 2022, **65**, 1362–1373.
75 M. Zhang, X. Guo, W. Ma, H. Ade and J. Hou, *Adv. Mater.*, 2015, **27**, 4655–4660.
76 K. Vandewal, J. Benduhn and V. C. Nikolis, *Sustainable Energy Fuels*, 2018, **2**, 538–544.
77 J. Yao, T. Kirchartz, M. S. Vezie, M. A. Faist, W. Gong, Z. He, H. Wu, J. Troughton, T. Watson, D. Bryant and J. Nelson, *Phys. Rev. Appl.*, 2015, **4**, 014020.
78 W. Shockley and H. J. Queisser, *J. Appl. Phys.*, 1961, **32**, 510–519.
79 K. Vandewal, K. Tvingstedt, A. Gadisa, O. Inganas and J. V. Manca, *Nat. Mater.*, 2009, **8**, 904–909.
80 V. C. Nikolis, J. Benduhn, F. Holzmueller, F. Piersimoni, M. Lau, O. Zeika, D. Neher, C. Koerner, D. Spoltore and K. Vandewal, *Adv. Energy Mater.*, 2017, **7**, 1700855.